Correspondence to:
S. Y. Fu,
suiyanfu@pku.edu.cn

Oxygen Ion Butterfly Distributions Observed in a Magnetotail Dipolarizing Flux Bundle

S. J. Zhao[1], S. Y. Fu[1], W. J. Sun[2], X. Z. Zhou[1], Z. Y. Pu[1], L. Xie[1], T. Wu[1], Y. Xiong[1], H. Zhang[1], Q. G. Zong[1], and F. B. Yu[1]

[1]School of Earth and Space Sciences, Peking University, Beijing, China, [2]Department of Climate and Space Sciences and Engineering, University of Michigan, Ann Arbor, MI, USA

Abstract Cluster observed two intermittent oxygen ion (O^+) flux enhancements with energy dispersions in a dipolarizing flux bundle, which is known as a region of enhanced northward magnetic field (B_z) embedded in the earthward high-speed flow. The flux enhancements of O^+ show clear pitch angle dependences, which are termed as butterfly distributions. Two corresponding flux enhancements of field-aligned protons (H^+) are also shown in its spectrum, but they are weaker and emerge later (~10 s) than those of O^+. Simulation shows that both enhanced ion species are the counterstreaming populations. They originated from the lobe region and were driven into the center plasma sheet by the dawn-dusk electric field (E_y). Backward tracing test-particle simulations reproduce the butterfly O^+ and the counterstreaming H^+ distribution. The differences between O^+ and H^+ are because of their different gyroradii. The lobe O^+ can arrive at the magnetic equatorial plane in less than one gyromotion due to its large gyroradius, and O^+ with a larger field-aligned velocity can arrive at the equatorial plane earlier, leading to the energy and pitch angle dependence. While H^+ with similar energy can drift into dipolarizing flux bundle through electric field drift ($\mathbf{E} \times \mathbf{B}$ motion) and arrive at the equatorial plane through adiabatic motion, which consequently forms the field-aligned flux enhancements in dipolarizing flux bundle, that is, the B_z-dominant region. The simulation further confirms that intermittent increases of E_y component can produce the two intermittent flux enhancements, as indicated in the in situ observation.

1. Introduction

Bursty bulk flows are known as a group of intermittent flow bursts transporting mass, energy, and magnetic flux from the magnetotail toward the inner magnetosphere (Angelopoulos et al., 1992, 1994). Near the leading edge of these flow bursts, a localized thin current sheet layer with an abrupt increase of northward magnetic field and decrease in plasma density is often observed, which is commonly denoted as dipolarization front (DF; e.g., Nakamura et al., 2002; Ohtani et al., 2004; Runov et al., 2009; Zhou et al., 2009). The DF has thickness comparable to background proton inertial length (~500 to ~1,000 km) and carries intense current with current densities of tens of nA/m^2 (e.g., Liu et al., 2013; Runov et al., 2009; Sun et al., 2013, 2014; Yao et al., 2013; Zhou et al., 2013). Following the DF, a structure containing a large amount of dipolarized magnetic flux and hot and tenuous reconnected plasmas is called dipolarizing flux bundle (DFB; Liu et al., 2013). The structure is embedded in bursty bulk flows and propagates earthward by interchange motions with ambient cold and dense plasma, which consists with the plasma bubble model (Chen & Wolf, 1999).

Ambient particles ahead of DF can cross DF and be accelerated and then reflected by convection electric field ($\mathbf{V} \times \mathbf{B}$) in DFB (e.g., Zhou et al., 2010, 2018). Observations and simulations confirmed this process by showing ion distribution in the plasma sheet ahead of DF containing both backgrounds and accelerated populations (e.g., Eastwood et al., 2015; Wu & Shay, 2012; Zhao et al., 2016; Zhou et al., 2010, 2011). Several studies further propose that energetic protons and electrons (tens of keV) from the plasma sheet boundary layers and the adjacent lobes may be picked up and transported to the inner magnetosphere by convection electric field associated with DFB (e.g., Birn et al., 2014; Gabrielse et al., 2012; Yang et al., 2011). In addition to ion distributions ahead of DF, ion distributions behind DF, that is, inside DFB, attracted a lot of attention recently. Eastwood et al. (2015) show counterstreaming ions in both observation and particle-in-cell simulation. They propose that the counterstreaming ions originate from the thermal ions in the outer plasma sheet ahead of DF. Runov et al. (2017) show that ions are anisotropy in the perpendicular direction in DFB, and Zhou et al. (2018) propose that the anisotropy is caused by multiple ion reflections.

In the studies mentioned above, H^+ is assumed to be the only ion species in the plasma sheet. How heavy ions (for instance, O^+) distributed in the DFBs are not clear. It is well known that the singly-charged oxygen ions (O^+) are originated from the ionosphere and could play an important role in the Earth's magnetospheric dynamics (e.g., Fu et al., 2001; Seki et al., 2001; Shay & Swisdak, 2004). They may influence the magnetotail reconnection in several aspects, such as reducing reconnection rate (e.g., Karimabadi et al., 2011; Markidis et al., 2011; Shay & Swisdak, 2004), slowing down reconnection exhaust (e.g., Liang et al., 2016), and forming a larger-scale diffusion region than those of merely protons (Liu et al., 2015). Wu et al. (2016) also show that O^+ can form thin current layers (smaller than half-thickness of the current sheet) in the reconnecting current sheet. Zhao et al. (2018) show that ambient O^+ ahead of DF can be accelerated and reflected by DFs as H^+, but they can reach a further position and exhibit an energy-dependent flux dropout in the spectrum, which highly depends on the gyromotion of O^+. Simulation works show that although O^+ has much larger gyroradii and may form a much larger diffusion region than that of protons, they still can be found counterstreaming in the exhaust (Liang et al., 2017). Tenfjord et al. (2018) report that O^+ can bounce between the Hall electric field in the separatrices. They could be trapped in the potential well of exhaust and develop into high-density layers. There are many unknowns about O^+ in the tail dynamics. More details on how O^+ enter the DFBs and similarities and differences between O^+ and H^+ need further investigation.

In this paper, we present an observation of two intermittent O^+ and H^+ flux enhancements in a DFB from Cluster measurements. In section 2, Cluster observations of the O^+ and H^+ flux enhancements are analyzed. The O^+ flux enhancements are energy and pitch angle dependences, and these populations are termed as butterfly O^+ based on the feature of pitch angle distributions. The H^+ flux enhancements are counterstreaming, appear later, and are weaker in intensity. In section 3, we reproduce the characteristics for both O^+ and H^+ by a backward tracing test-particle Liouville simulation. It suggests that the distinct signatures between O^+ and H^+ arise from different gyroradius. Discussion and conclusion are in sections 4 and 5, respectively.
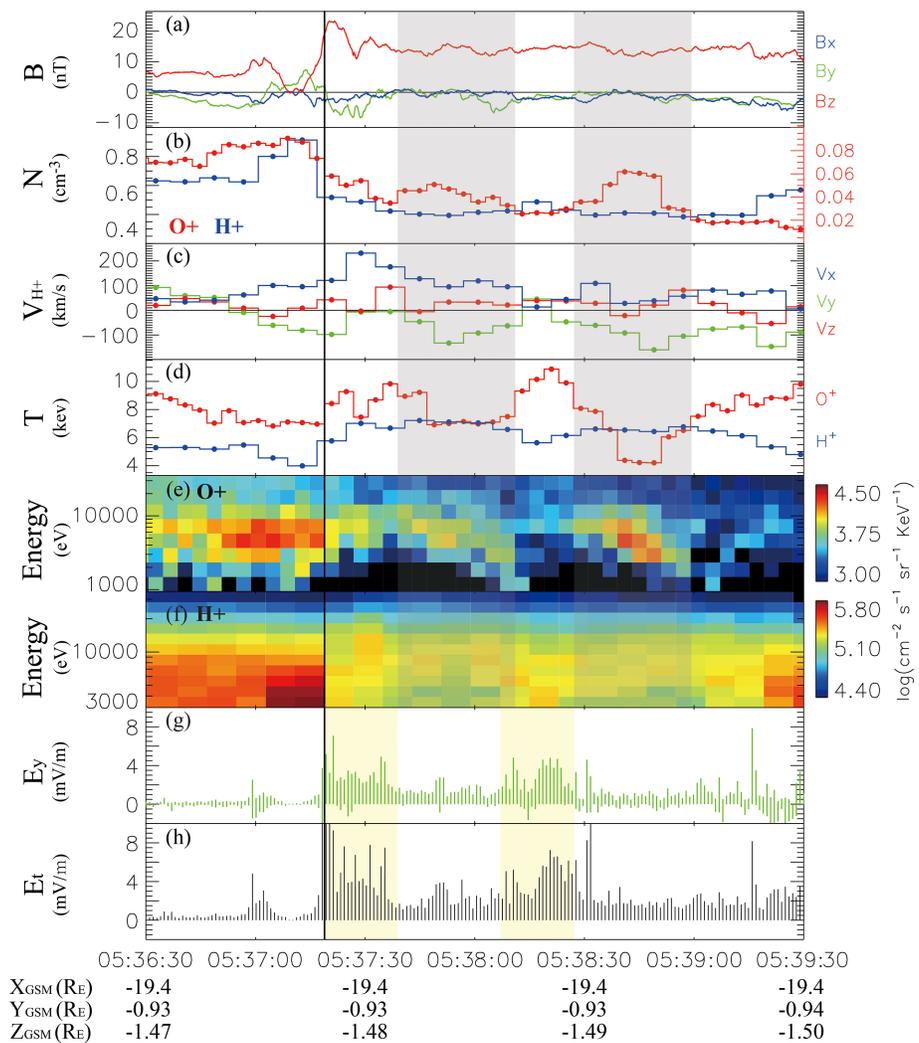
2. Observations

2.1. Data Set

This study employs data obtained from instruments onboard Cluster (Escoubet et al., 2001). The fluxgate magnetometer provides magnetic field measurements with a full resolution of ~22.5 Hz (Balogh et al., 2001). Ion data are from the ion composition and distribution function analyzer (CODIF), which is part of the ion spectrometry (CIS) experiment (Rème et al., 2001). The CODIF can resolve ions, including H^+, He^{2+}, He^+, and O^+, through the time of flight, and provides distribution functions in an energy range from ~25 eV to ~40 keV every spin (4 s). However, the calibrated data may usually be of lower resolution (>4 s). The electric field is measured by the electric field and wave instrument (Gustafsson et al., 2001) with a sampling frequency of 25 Hz. We present all data in the Geocentric Solar Magnetospheric coordinate system in this paper unless otherwise specified.

2.2. Event on 2 September 2002

Figure 1 shows a DFB observed by Cluster 4 (C4) on 2 September 2002 when Cluster was located at X_{GSM}~ $-19 R_E$. The leading edge of the DFB was identified as a DF, which corresponded to a B_z increase of ~15 nT in less than 10 s and was preceded by a B_z dip (Figure 1a). The vertical black line in Figure 1 represents the point when the northward magnetic field (B_z) had the largest increase slope (~05:37:19 UT). C4 was located in the central plasma sheet ($\beta > 0.5$; not shown) before crossed the DF. In the magnetic dip region, H^+ number density (N_{H+}) increased (Figure 1b), and H^+ velocity (V_{H+}) started to increase (Figure 1c). After entered the DFB, N_{H+} quickly decreased from ~0.8 to ~0.5 cm^{-3}, which was lower than density of the ambient plasma sheet (~0.65 cm^{-3}), and H^+ temperature (T_{H+}) increased from ~4 to ~6 keV (Figure 1d). The V_{H+} gradually reached to a maximum of ~200 km/s. In the DFB, the B_z was stable and maintained at a high value of ~15 nT in ~2 min. The parameters of O^+ exhibited similar variations as the H^+. However, an increase of N_{O+} ahead of the DF and a decrease of N_{O+} in the DFB were more gradual than those of N_{H+}, which is consistent with the features of O^+ around DF investigated in Zhao et al. (2018).

Figure 1. Overview of field and ion observations from Cluster-4 for the dipolarization front (DF) on 2 September 2002. (a) Magnetic field components, B_x (blue), B_y (green), B_z (red); (b) O$^+$ and H$^+$ density, N_{O+} (red), N_{H+} (blue); (c) H$^+$ velocity components, V_x (blue), V_y (green), V_z (red); (d) ion temperature, T_{O+} (red), T_{H+} (blue); (e) O$^+$ and (f) H$^+$ energy spectrum for differential particle flux; (g) E_y component and (h) total intensity of electric field. The black vertical line indicates the DF where B_z has the largest slope, the gray shadows indicate the durations of O$^+$ flux enhancements, and the yellow shadows indicate the durations when E_y increased.

In the DFB, two intermittent flux enhancements of O$^+$ were shown up in the energy spectrum (Figure 1e) from 05:37:39 UT to 05:38:11 UT and from 05:38:27 UT to 05:38:59 UT (highlighted in gray regions), which were accompanied with N_{O+} increases (Figure 1b) and T_{O+} decreases (Figure 1d). The O$^+$ flux enhancements were dispersed, showing that the higher-energy O$^+$ appeared earlier and the lower energy O$^+$ appeared later. In the periods of O$^+$ flux enhancements, the H$^+$ energy spectrum (Figure 1f), N_{H+} (Figure 1b), and T_{H+} did not show clear variations, which were different from the O$^+$. Figures 1g and 1h show the dawn-dusk component (E_y) and total value (E_t) of the electric field, respectively. The E_y was comparable with the E_t, indicating that the E_y was the main component. The E_y enhanced to ~3 mV/m from 05:37:19 UT to 05:37:39 UT and from 05:38:07 UT to 05:38:27 UT (marked by yellow shadows) in the DFB, which are ~20 s earlier than the O$^+$ flux enhancements separately.

In this period, Cluster 1 (C1) observed similar variations of H$^+$ and O$^+$ associated with the DFB (not shown). However, the CODIF time resolution was lower (~8 s) than C4. C2 and C3 did not provide CODIF measurements in that period. We performed an analysis of the spectra of O$^+$ and H$^+$ from C4 in the next section to investigate the features of the O$^+$ flux enhancements.
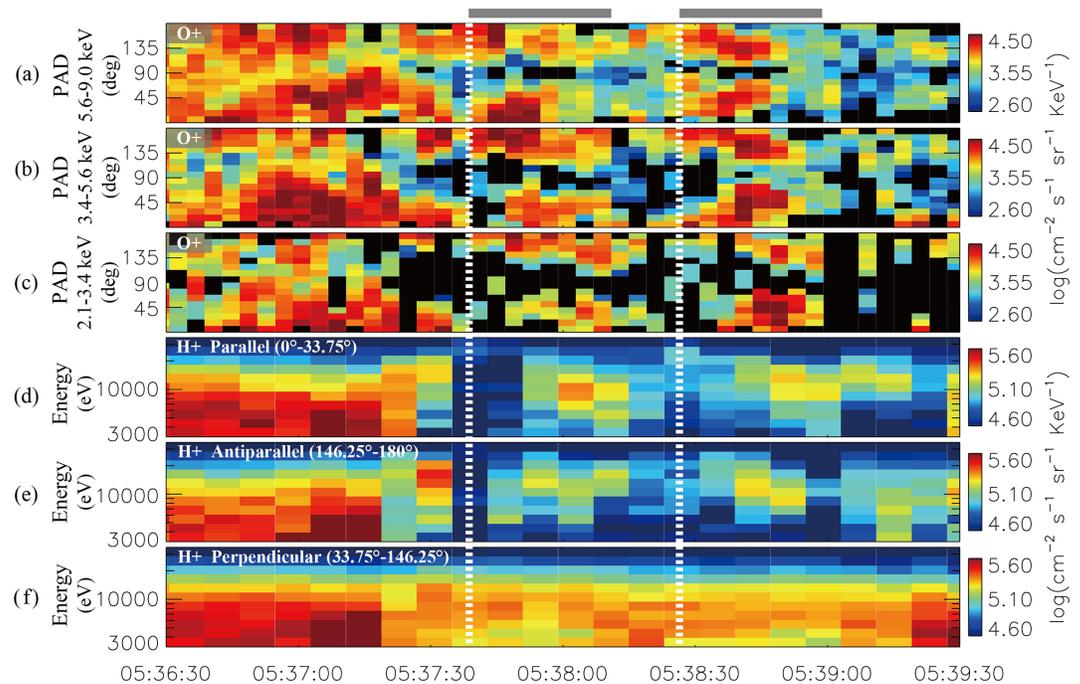
Figure 2. Observations of the O^+ and H^+ flux enhancements. O^+ pitch angle distributions in the energy range: (a) from ~5.6 to ~9.0 keV, (b) from ~3.4 to ~5.6 keV, and (c) from ~2.1 to ~3.4 keV; H^+ energy spectra of the differential particle flux in the pitch angle range: (d) from 0° to 33.75°, (e) from 146.25° to 180°, and (f) from 33.75° to 146.25°. The gray segments on the top mark the main durations of O^+ flux enhancements, corresponding to the gray shadow durations in Figure 1. The white vertical lines indicate the start times of each O^+ flux enhancements.

2.3. Butterfly Distributions of O^+ in DFB

Figures 2a–2c present O^+ pitch angle distributions with energy ranging from 2.1 to 9.0 keV, which includes the main energy range of the O^+ flux enhancements in Figure 1. Each panel contains two energy channels of CODIF. Gray segments on the top of the figure correspond to the gray shaded durations in Figure 1, and vertical dotted lines indicate the start times of the O^+ flux enhancements. In each enhancement, O^+ in the parallel and the antiparallel directions appeared first, and then the O^+ with pitch angles toward the perpendicular direction. This O^+ distribution can be described as butterfly distributions. The pith angle distributions suggest that, in addition to energy dependences, the O^+ flux enhancements also contain pitch angle dependences.

Considering that the B_x was very small (~0 nT) and the magnetic field direction is mainly northward during the interval, C4 was located in the central region of the plasma sheet, which is at or near the magnetic equatorial plane. The O^+ flux enhancements incorporate cold populations from both northward and southward (i.e., counterstreaming populations), which are distinct to the hot, tenuous, and earthward reconnection outflows inside DFB. More interestingly, the populations from northward and southward were showed up and disappeared almost simultaneously.

As shown in Figure 1, the H^+ energy spectrum did not show clear flux enhancements (Figure 1f). However, due to a lower flux of the enhanced H^+, they could mix with the earthward propagating populations, which are mainly distributed in the perpendicular direction in the central DFB. Thus, Figures 2d–2f show the H^+ energy spectra in parallel (pitch angles ranging from 0° to 33.75°), antiparallel (pitch angles ranging from 146.25° to 180°), and perpendicular directions (pitch angles ranging from 33.75° to 146.25°), respectively. Indeed, two flux enhancements were shown up in both parallel and antiparallel spectra. However, the energy dependences are not as obvious as O^+, which could because of the lower time resolution of H^+ measurements (~8 s). Furthermore, the H^+ flux enhancements have similar durations (~30 s) as the O^+ flux enhancements but appeared slightly later (comparing to the vertical dotted lines) with time delays of ~10 s. In the perpendicular direction (Figure 2f), the flux was higher than

those in parallel and antiparallel directions, but the energy spectrum did not contain clear flux enhancement.

In a summary of the observation, two intermittent O^+ and H^+ flux enhancements were observed in the DFB. The O^+ flux enhancements show clear energy dispersion with the higher-energy O^+ appearing earlier and then the lower energy O^+. Further analysis shows that they are also pitch angle dependence, in which O^+ in the parallel and the antiparallel directions appeared first and then gradually deflecting to the perpendicular direction. Meanwhile, the H^+ flux shows enhancements in the parallel and antiparallel directions, but the enhancements appeared ~10 s later than the O^+ flux enhancements. In the next section, we investigate the O^+ and H^+ distributions in DFBs using a test particle simulation to seek the mechanisms responsible for those enhancements.

3. Test-Particle Simulations

In this section, we applied a backward tracing test-particle simulation (Zhao et al., 2018; Zhou et al., 2011, 2014) to study the features of butterfly O^+ and counterstreaming H^+. In the simulation, the first step is to set an initial ion distributions $f(r_i, v_i, t_i)$ in a DFB model. For the distributions $f(r, v, t)$ at any time t, it is easy to obtain their corresponding locations r_i and velocities v_i at t_i by tracing the ion trajectories backward in time. Then the phase space density $f(r, v, t)$ is determined by equaling to $f(r_i, v_i, t_i)$ according to Liouville's theorem (e.g., Schwartz, 1998; Wanliss et al., 2002).

Magnetic field of the DFB model consists of a background magnetic field and an earthward propagating DF-associated field. A two-dimensional (y independent) plasma sheet model (e.g., Harris, 1962; Pritchett & Coroniti, 1995) is adopted to model the finite background magnetic field in the magnetotail, which was applied in several previous works (Zhao et al., 2018; Zhou et al., 2014). The magnetic field and plasma density distributions of the initial equilibrium model can be seen in Zhou et al. (2014). The magnetic field has divergence equal to zero everywhere in the model. The virtual spacecraft was placed in the central plasma sheet at $r_0 (x_0, y_0, z_0) = (-19, 0, 0) R_E$, according to the Cluster location in the case. The model parameters are very similar to those used in Zhao et al. (2018). Some parameters included L, the half-thickness of the plasma sheet, equals 0.5 R_E; B_n, the B_z at the neutral sheet, equals 2 nT (equatorial B_z gradient is removed here for simplifying); B_0, the lobe magnetic field strength at x_0, equals to 30 nT. An earthward propagating DF-associated electromagnetic field was superposed over the initial background, and the DFB region is featured by a B_z enhancement which is given by

$$B_z(x, y, t) = \frac{B_f}{2}\left[1 - tanh\left(\frac{x^*}{L_f}\right)\right]exp\left(-\frac{y^2}{H_f{}^2}\right),$$

where $x^* = x - x_f - v_f(t - t_i)$ indicates a speed of v_f, the max value of which equals 200 km/s, in consistent with the protons v_x near the DF in observation (Figure 1c). Here, B_f, the B_z enhancement of DFB, equals to 15 nT; L_f, the DF half-thickness, equals to 0.1 R_E; H_f, the half-width of DFB in y direction, equals to 2 R_E; and x_f, the initial x location of DF at $t = t_i$, equals to 18 R_E. The dawn-dusk electric field associated with the DFB was calculated through the Faraday's law

$$E_y(x, y, t) = v_f B_z(x, y, t),$$

which is always perpendicular to the magnetic field and independent of z. Since the electric field is not divergence-free, the assumption requires that the DF is charged positively on the dawnside and negatively on the duskside, which is qualitatively consistent with the plasma bubble model (Pontius & Wolf, 1990; Wolf et al., 2009). Therefore, the electric field can be considered as a superposition of an induced and a static potential electric field (see more details in Zhou et al. (2014)). This E_y with a maximum equaling to 3 mV/m is comparable to the observed E_y (Figure 1g). Moreover, because the observed E_y enhancement was intermittent, we set that the E_y only lasts ~25 s from $t = t_i$ in the simulation to match the observational feature. Since B_z is constant in the DFB region in our model, the E_y variation can be considered as a change of v_f. The following simple linear change is used:
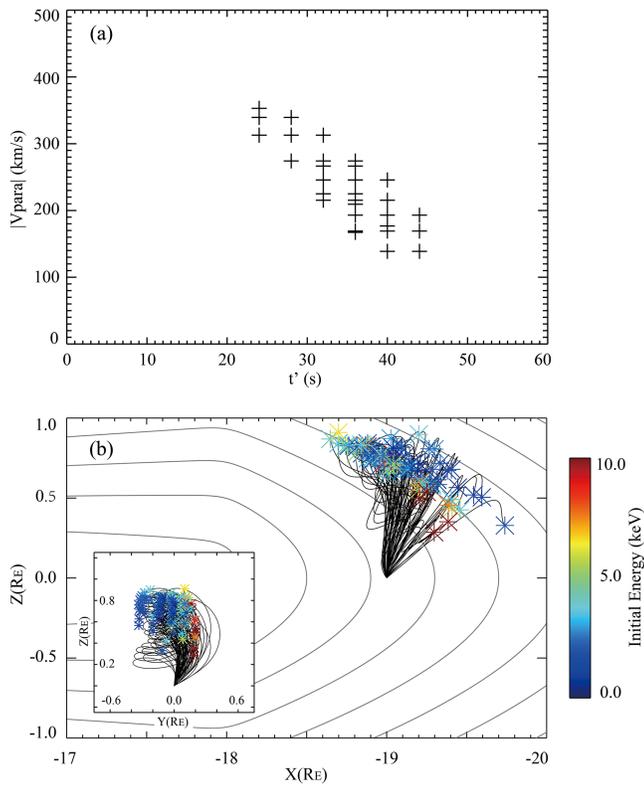
Figure 3. On the typical test particles selected from observed O^+ butterfly population in the duration from 05:38:27 UT to 05:38:59 UT. (a) Selected test particles are plotted in$|V_{para}|$-t′ plane, where t′ = t − t_i and t_i equals to the beginning time of E_y increasing (05:38:07). (b) Typical orbits of the selected O^+, the asterisks mark their initial position with the color indicating the initial energy.

$$\begin{cases} v_f(t) = 200 \; km/s & t_i{\leq}t{<}t_i + 20s \\ v_f(t) = 1000{-}40(t{-}t_i) \; km/s & t_i + 20s{\leq}t{<}t_i + 25s \\ v_f(t) = 0 \; km/s & t{\geq}t_i + 25s \end{cases}$$

here $E_y(t) = v_f(t)B_z(t)$ also satisfies the Faraday's law. The E_y field experienced by particles in the region behind DF is shown in Figure 4a.

Based on the DFB model, we can select the typical particles in the O^+ enhancement and backward trace them to the source region. Figure 3a shows the test particles chosen from the O^+ spectrum in the second flux enhancement (from 05:38:27 UT to 05:38:59 UT in Figures 1e and 2a–2c, southward O^+). The bins with significant fluxes were shown in the |V_{para}|-t′ plane, where |V_{para}| is the intensity of O^+ field-aligned velocity and t′ equals to t − t_i. We define the start of E_y increasing as the beginning time (t_i = 05:38:07 UT). The field-aligned velocity and the time are anti-correlated. Figure 3b shows the trajectories of these O^+ test particles in x-z plane and y-z plane. The asterisks mark the initial positions of test particles, and the color indicates their initial energy. The gray lines represent the magnetic field lines at y = 0 and t = t_i. The field lines are essentially a superposition of the background field of the two-dimensional plasma sheet model and B_z of the DF. It can be seen that most of the ions came from the high-latitude region with lower energy. They entered the central plasma sheet from the northside in less than one gyroradius. This result implies that the source of the butterfly O^+ is the lobe-featured ions from high-latitude region. With this result, we then show distributions of the lobe-originated populations, and further investigate the mechanism responsible for the formation of butterfly O^+ and compare the differences between O^+ and H^+ distributions.

Figure 4e shows the topology of magnetic fields at y = 0 and t = t_i (t_i = 0 in this run), and the location of the virtual satellite is marked by the red point in the plot. The red shadows indicate the source regions in the y = 0 plane, which are marked according to the result in Figure 3b. The boundary is a combination of the DF surface, plasma sheet boundary (|z|= 0.5 R_E), and the field line crossing the (x, z) = (−19.7, 0) R_E (this part can be simply considered as the separatrices between DFB and inflow region). We assumed that there were no initial distributions in other regions by setting f (r$_i$, v$_i$, t$_i$) = 0. The hot populations preexisting in the central DFB (which may be related to the bursty bulk flows and reconnections) and the ambient populations that crossed DF were ignored. Based on the two-dimensional plasma sheet equilibrium with Maxwellian ion distributions (more details in Zhou et al. (2018, 2011)), a cold (v$_T$ = 400 km/s for H^+ and v$_T$ = 100 km/s for O^+), tenuous (n$_0$ = 0.1 cm^{-3}), and nondrifting population was superposed over the source region to represent the background plasma and the lobe limit, where n$_0$ is the plasma density and v$_T$ is the ion thermal velocity. It should be mentioned that the excluding ions originating from other regions would not influence the entry process of lobe populations. Furthermore, the exclusion can make the features that we focus on more prominent.

Figures 4b and 4c show the simulated energy spectrum and the simulated pitch angle distribution of O^+, respectively. They can represent the observations from the virtual satellite. The differential energy flux in each bin is normalized by the initial energy flux of O^+ of ~1 keV in the source region at (−19, 0, 1) R_E. Initial energy flux means the differential energy flux at t = t_i (i.e., t = 0). The flux enhancements begin to appear at t~18 s and last ~30 s. Both energy dependence (Figure 4b) and pitch angle dependence (Figure 4c) were shown up which are consistent with the observations.

Figures 4f and 4g show two typical orbits of O^+ (P1 and P2, respectively) in the energy flux enhancements. P1 corresponds to the black point with a higher energy and a field-aligned pitch angle in Figures 4b and 4c, which represents the early appeared O^+. P2 corresponds to the red point with a lower energy and a pitch
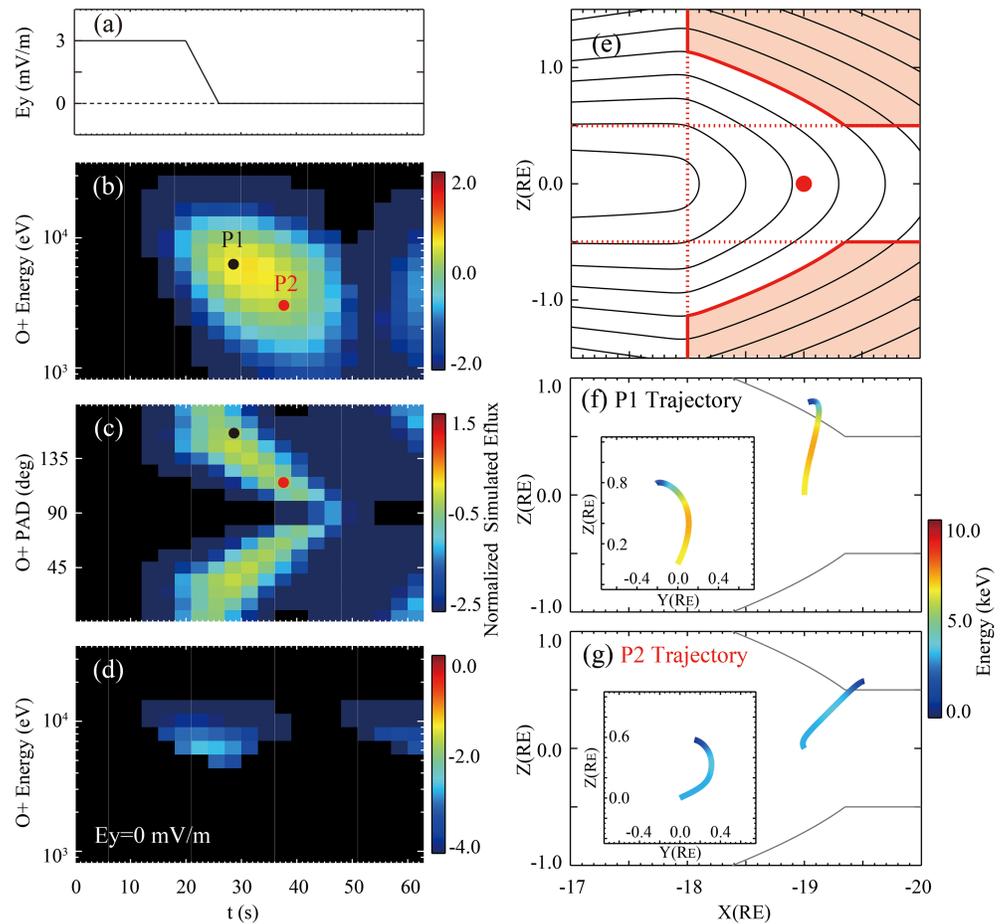
Figure 4. Simulated results of butterfly O^+. (a) E_y electric field. (b) Simulated energy spectrum and (c) pitch angle distribution of O^+ under the condition with E_y shown in Figure 4a. (d) Simulated O^+ energy spectrum under the condition that $E_y = 0$. (e) Magnetic field lines in the y-z plane at $t = 0$; the red point marks the location of the virtual satellite, the red shadows indicate the source regions, the vertical dotted line indicates the DF, and the horizontal dotted lines indicate the boundary of plasma sheet. (f and g) Typical orbits of O^+ at the locations corresponding to the black point and red point in Figures 4b and 4c; the color indicates the particles energy.

angle closer to 90°, which represents the later appeared O^+. The colors on the lines indicate the energies of the particles. The P1 and the P2 have a similar initial energy (~1 keV). When they encountered the enhanced E_y region, they were accelerated in y direction, and then crossed the separatrices and arrived at the central plasma sheet. These processes occurred in less than one gyroperiod due to the large gyroradii of O^+. Comparing the trajectories of P1 and P2, we can find that once O^+ crossed the separatrices and entered the B_z-dominant region, P1, which had a higher field-aligned velocity, would arrive at the central plasma sheet earlier. Consequently, it would produce the energy dependence and the pitch angle dependence of O^+. To validate the contributions of E_y, Figure 4d shows the energy spectrum of O^+ by running the model with $V_f = 0$ km/s ($E_y = 0$), in which the entry of lobe O^+ was not effective and energy and pitch angle dependences were not clear. Therefore, we conclude that the E_y field plays an important role in the formation of butterfly O^+. It also should be mentioned that ions observed in Figure 4d usually have a lager initial energy and their trajectories are similar to those of P1 and P2 (not shown).

Figures 5a and 5b show the simulated energy spectrum and pitch angle distribution of H^+, which can be understood as observations of our virtual satellite at $(-19, 0, 0)$ R_E. The energy flux is also normalized by the initial energy flux ($t = 0$ s) of H^+ with energy ~1 keV at $(-19, 0, 1)$ R_E. The protons presented flux enhancement in Figure 5a. However, the enhancement appeared later (with a time delay ~10 s), and entry efficiency is lower than those of O^+. Furthermore, the H^+ mainly concentrated around pitch angles of ~145° and ~35°
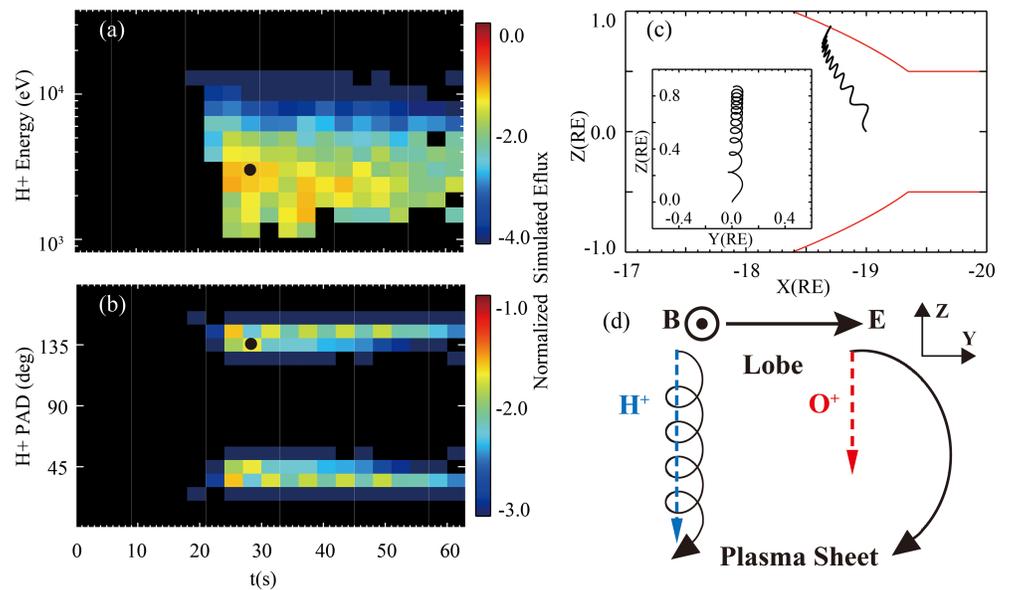
Figure 5. On the differences between O^+ and H^+ flux enhancements. (a) Simulated energy spectrum and (b) pitch angle distribution of H^+. (c) Typical orbits of H^+ at the location corresponding to the black point in Figures 5a and 5b. (d) Schematic illustration of the O^+ and H^+ trajectories of crossing the plasma sheet boundary in northern hemisphere.

with no clear pitch angle dependence. The H^+ enhancements in quasi-parallel and quasi-antiparallel directions are consistent with the observed enhancements of field-aligned H^+ shown in Figure 2. However, because Cluster observed the mixture of both high-speed flow population and this enhanced population, it is difficult to separate the two and, therefore, make more detailed comparisons between lobe-originated H^+ features in simulated and observed pitch angle distributions. An orbit of a typical H^+ in the energy flux enhancement, which corresponds to the black points in Figures 5a and 5b, is displayed in Figure 5c. Similar to the O^+, H^+ crossed the separatrices and drifted into the B_z-enhanced region under the influence of the E_y. However, O^+ reached the central plasma sheet in less than one gyroradius, while H^+ needed much more gyroperiods due to its small gyroradius. Then, once H^+ entered the B_z-dominant region, they can approach the equatorial plane through an adiabatic motion along the field line. During this process, the magnetic field decreases and H^+ will gradually deflect to the parallel (antiparallel) direction due to the conservation of first adiabatic invariant ($\mu = W_\perp/B$). As a result, counterstreaming protons appeared in the plasma sheet. Birn et al. (2017) also revealed this process, and they further pointed out that there was a slingshot effect which akin to first-order Fermi acceleration (Northrop, 1963) when H^+ approached the central plasma sheet. The observed counterstreaming populations are distributed closer to the parallel ($\sim0°$) and antiparallel direction ($\sim180°$) than that of simulation ($\sim35°$ and $\sim145°$, respectively), indicating that protons may experience a larger $\nabla_\parallel B$ in the real situation.

4. Discussion

The test particle simulations suggest that the dawn-dusk electric field (E_y) plays an important role for both O^+ and H^+ to enter from the lobe into the DFB. The flux enhancement of counterstreaming H^+ is later than that of butterfly O^+ with the same energy in both observations and simulations. H^+ drifts into the DFB by $\mathbf{E} \times \mathbf{B}$ motion, while O^+ can arrive at the equatorial plane directly in one gyromotion. Their separatrices crossing in the northern hemisphere are schematically illustrated in Figure 5d (not representing actual gyroradius ratio of O^+ and H^+ with the same energies, the electromagnetic field is uniform for simplification). It is easy to find that O^+ velocity toward the equatorial plane is much larger than the $\mathbf{E} \times \mathbf{B}$ drift speed, while H^+ velocity toward the equatorial plane is close to the $\mathbf{E} \times \mathbf{B}$ drift speed. Thus, the O^+ would approach the magnetic equatorial plane more quickly than the H^+.

Previous works have suggested that there are two sources for counterstreaming H^+ in DFBs. One is the preexisting H^+ in the outer plasma sheet ahead of DF (e.g., Eastwood et al., 2015); the other is H^+ in the lobe (or

the plasma sheet boundary layer; e.g., Birn et al., 2017). In the study of Eastwood et al. (2015), the counterstreaming H^+ shows up in a discrete region attached to the DF. While in this study, two intermittent counterstreaming populations, including H^+ and O^+, appeared further behind the DF, which is different from their results. Our test particle simulations suggest that the counterstreaming H^+ and O^+ are originated from the lobes, similar to the Birn et al. (2017). The lobe ions cross the separatrices from the inflow region, and they are accelerated by the enhanced dawn-dusk electric fields in the DFBs.

Another important feature in the observation is that there are two intermittent O^+ and H^+ enhancements in the DFB. It is interesting to know how the two intermittent flux enhancements are formed. Some recent studies proposed that the Hall electric field (E_z) around the separatrices can play an important role in the formation of counterstreaming O^+ in the reconnection outflow region (Liang et al., 2017; Tenfjord et al., 2018). Tenfjord et al. (2018) proposed that O^+ can bounce between the outflow boundaries, namely, the separatrices, forming high-density O^+ layers. Based on this scenario, the two intermittent flux enhancements in our case might be the same O^+ population bouncing between the separatrices. However, if the second enhancement is formed by bouncing O^+ from first enhancement, the slope of the second dispersion in energy flux spectrum should be smaller than that of the first dispersion (verified by a simple model; not shown). However, in C4 observation, the slopes of the two O^+ flux enhancements in the energy spectrum are similar. Therefore, it seems that the bouncing motion of the high-density O^+ layer is not the explanation of these two intermittent O^+ flux enhancements.

We propose that the two intermittent flux enhancements are more likely caused by the enhancements in the E_y field. Figure 1 shows that the two flux enhancements are both preceded by E_y increases. The E_y plays a key role in the formation of counterstreaming populations, and the O^+ flux enhancement is observed ~20 s later than the E_y increase, which are both reproduced in the simulation. It is possible that the two E_y increase causes two particle flux enhancements with similar features. However, the spacecraft only shows measurements in the central plasma sheet, and the electric field in the source region is unknown. This interpretation is based on an assumption that the E_y in the source region is similar to the measured electric field. Furthermore, the origin of the E_y is unknown, which might be associated with magnetic reconnection.

5. Summary

Cluster observations in combination with test-particle simulations have investigated two intermittent butterfly O^+ and counterstreaming H^+ in a DFB. The main conclusions are summarized as follows:

1. Two intermittent O^+ and H^+ flux enhancements are observed near the magnetic equatorial plane of a DFB. The O^+ flux enhancements are characterized by clear energy and pitch angle dependences, and these populations are termed as butterfly O^+ based on the feature of pitch angle distributions. The corresponding H^+ flux enhancements concentrate in the parallel and the antiparallel directions, which are called as counterstreaming H^+. The counterstreaming H^+ are weaker in flux enhancements and emerge later (~10 s) than those of the butterfly O^+.
2. The dawn-dusk electric field (E_y) plays a key role in the formation of butterfly O^+. Under the influence of the E_y, the lobe-originated O^+ cross the separatrices and arrive at the magnetic equatorial plane in less than one gyromotion. The O^+ of higher field-aligned velocity can arrive at the equatorial plane earlier. Consequently, it would result in the energy dependence and the pitch angle dependence of O^+. The two intermittent butterfly distributions are most likely associated with the two increases of E_y.
3. The lobe H^+ also crosses the separatrices by $\mathbf{E} \times \mathbf{B}$ motion. Then the H^+ can approach the magnetic equatorial plane through an adiabatic motion with the conservation of first adiabatic invariant. During this process, the magnetic field decreases and H^+ gradually deflect to the filed-aligned directions, producing the counterstreaming H^+ flux enhancements. In addition, H^+ flux enhancements appeared later than the O^+. It could be due to that O^+ can approach the equatorial plane more directly than H^+, during which O^+ velocity toward the equatorial plane is much higher than the guiding center speed of H^+.

References

Angelopoulos, V., Baumjohann, W., Kennel, C. F., Coroniti, F. V., Kivelson, M. G., Pellat, R., et al. (1992). Bursty bulk flows in the inner central plasma sheet. *Journal of Geophysical Research*, *97*(A4), 4027–4039.

Angelopoulos, V., Kennel, C. F., Coroniti, F. V., Pellat, R., Kivelson, M. G., Walker, R. J., et al. (1994). Statistical characteristics of bursty bulk flow events. *Journal of Geophysical Research*, *99*(A11), 21,257–21,280.

Balogh, A., Carr, C. M., Acuña, M. H., Dunlop, M. W., Beek, T. J., Brown, P., et al. (2001). The Cluster magnetic field investigation: Overview of in-flight performance and initial results. *Annales de Geophysique*, *19*(10/12), 1207–1217. https://doi.org/10.5194/angeo-19-1207-2001

Birn, J., Runov, A., & Hesse, M. (2014). Energetic electrons in dipolarization events: Spatial properties and anisotropy. *Journal of Geophysical Research: Space Physics*, *119*, 3604–3616. https://doi.org/10.1002/2013JA019738

Birn, J., Runov, A., & Zhou, X.-Z. (2017). Ion velocity distributions in dipolarization events: Distributions in the central plasma sheet. *Journal of Geophysical Research: Space Physics*, *122*, 8014–8025. https://doi.org/10.1002/2017JA024230

Chen, C. X., & Wolf, R. A. (1999). Theory of thin-filament motion in Earth's magnetotail and its application to bursty bulk flows. *Journal of Geophysical Research*, *104*(A7), 14,613–14,626. https://doi.org/10.1029/1999JA900005

Eastwood, J. P., Goldman, M. V., Hietala, H., Newman, D. L., Mistry, R., & Lapenta, G. (2015). Ion reflection and acceleration near magnetotail dipolarization fronts associated with magnetic reconnection. *Journal of Geophysical Research: Space Physics*, *120*, 511–525. https://doi.org/10.1002/2014JA020516

Escoubet, C. P., Fehringer, M., & Goldstein, M. (2001). Introduction: The Cluster mission. *Annales de Geophysique*, *19*, 1197–1200.

Fu, S. Y., Wilken, B., Zong, Q.-G., & Pu, Z. Y. (2001). Ion composition variation in the inner magnetosphere-individual and collective storm effects in 1991. *Journal of Geophysical Research*, *106*, 29,683–29,698.

Gabrielse, C., Angelopoulos, V., Runov, A., & Turner, D. (2012). The effects of transient, localized electric fields in equatorial particle acceleration and transport towards the inner magnetosphere. *Journal of Geophysical Research*, *117*, A10213. https://doi.org/10.1029/2012JA017873

Gustafsson, G., André, M., Carozzi, T., Eriksson, A. I., Fälthammar, C. G., Grard, R., et al. (2001). First results of electric field and density observations by Cluster EFW based on initial months of operation. *Annales de Geophysique*, *19*(10/12), 1219–1240. https://doi.org/10.5194/angeo-19-1219-2001

Harris, E. G. (1962). On a plasma sheet separating regions of oppositely directed magnetic field. *Nuovo Cimento*, *23*, 115–121.

Karimabadi, H., Roytershteyn, V., Mouikis, C. G., Kistler, L. M., & Daughton, W. (2011). Flushing effect in reconnection: Effects of minority species of oxygen ions. *Planetary and Space Science*, *59*(7), 526–536. https://doi.org/10.1016/j.pss.2010.07.014

Liang, H., Ashour-Abdalla, M., Lapenta, G., & Walker, R. J. (2016). Oxygen impacts on dipolarization fronts and reconnection rate. *Journal of Geophysical Research: Space Physics*, *121*, 1148–1166. https://doi.org/10.1002/2015JA021747

Liang, H., Lapenta, G., Walker, R. J., Schriver, D., El-Alaoui, M., & Berchem, J. (2017). Oxygen acceleration in magnetotail reconnection. *Journal of Geophysical Research: Space Physics*, *122*, 618–639. https://doi.org/10.1002/2016JA023060

Liu, J., Angelopoulos, V., Runov, A., & Zhou, X.-Z. (2013). On the current sheets surrounding dipolarizing flux bundles in the magnetotail: The case for wedgelets. *Journal of Geophysical Research: Space Physics*, *118*, 2000–2020. https://doi.org/10.1002/jgra.50092

Liu, Y. H., Mouikis, C. G., Kistler, L. M., Wang, S., Roytershteyn, V., & Karimabadi, H. (2015). The heavy ion diffusion region in magnetic reconnection in the Earth's magnetotail. *Journal of Geophysical Research: Space Physics*, *120*, 3535–3551. https://doi.org/10.1002/2015JA020982

Markidis, S., Lapenta, G., Bettarini, L., Goldman, M., Newman, D., & Andersson, L. (2011). Kinetic simulations of magnetic reconnection in presence of a background O^+ population. *Journal of Geophysical Research*, *116*, A00K16. https://doi.org/10.1029/2011JA016429

Nakamura, R., Baumjohann, W., Klecker, B., Bogdanova, Y., Balogh, A., Rème, H., et al. (2002). Motion of the dipolarization front during a flow burst event observed by Cluster. *Geophysical Research Letters*, *29*(20), 1942. https://doi.org/10.1029/2002GL015763

Northrop, T. G. (1963). *The adiabatic motion of charged particles*. New York: Interscience.

Ohtani, S. I., Shay, M. A., & Mukai, T. (2004). Temporal structure of the fast convective flow in the plasma sheet: Comparison between observations and two-fluid simulations. *Journal of Geophysical Research*, *109*, A03210. https://doi.org/10.1029/2003JA010002

Pontius, D. H., & Wolf, R. A. (1990). Transient flux tubes in the terrestrial magnetosphere. *Geophysical Research Letters*, *17*, 49–53.

Pritchett, P. L., & Coroniti, F. V. (1995). Formation of thin current sheets during plasma sheet convection. *Journal of Geophysical Research*, *100*(A12), 23,551–23,565. https://doi.org/10.1029/95JA02540

Rème, H., Aoustin, C., Bosqued, J. M., Dandouras, I., Lavraud, B., Sauvaud, J. A., et al. (2001). First multispacecraft ion measurements in and near the Earth's magnetosphere with the identical Cluster ion spectrometry (CIS) experiment. *Annales de Geophysique*, *19*(10/12), 1303–1354. https://doi.org/10.5194/angeo-19-1303-2001

Runov, A., Angelopoulos, V., Artemyev, A., Birn, J., Pritchett, P. L., & Zhou, X.-Z. (2017). Characteristics of ion distribution functions in dipolarizing flux bundles: Event studies. *Journal of Geophysical Research: Space Physics*, *122*, 5965–5978. https://doi.org/10.1002/2017JA024010

Runov, A., Angelopoulos, V., Sitnov, M. I., Sergeev, V. A., Bonnell, J., McFadden, J. P., et al. (2009). THEMIS observations of an earthward-propagating dipolarization front. *Geophysical Research Letters*, *36*, L14106. https://doi.org/10.1029/2009GL038980

Schwartz, S. J. (1998). Shock and discontinuity normals, Mach numbers and related parameters. In G. Paschmann, & P. W. Daly (Eds.), *Analysis methods for multi-spacecraft data*, (pp. 249–270). Bern, German: Int. Space Sci. Inst.

Seki, K., Elphic, R. C., Hirahara, M., Terasawa, T., & Mukai, T. (2001). On atmospheric loss of oxygen ions from Earth through magnetospheric processes. *Science*, *291*(5510), 1939–1941. https://doi.org/10.1126/science.1058913

Shay, M. A., & Swisdak, M. (2004). Three-species collisionless reconnection: Effect of O^+ on magnetotail reconnection. *Physical Review Letters*, *93*(17), 175001. https://doi.org/10.1103/PhysRevLett.93.175001

Sun, W. J., Fu, S., Pu, Z., Parks, G. K., Slavin, J. A., Yao, Z., et al. (2014). The current system associated with the boundary of plasma bubbles. *Geophysical Research Letters*, *41*, 8169–8175. https://doi.org/10.1002/2014GL062171

Sun, W. J., Fu, S. Y., Parks, G. K., Liu, J., Yao, Z. H., Shi, Q. Q., et al. (2013). Field-aligned currents associated with dipolarization fronts. *Geophysical Research Letters*, *40*, 4503–4508. https://doi.org/10.1002/grl.50902

Tenfjord, P., Hesse, M., & Norgren, C. (2018). The formation of an oxygen wave by magnetic reconnection. *Journal of Geophysical Research: Space Physics*, *123*, 9370–9380. https://doi.org/10.1029/2018JA026026

Wanliss, J. A., Sydora, R. D., Rostoker, G., & Rankin, R. (2002). Origin of some anisotropic tailward flows in the plasma sheet. *Annales de Geophysique*, *20*(10), 1559–1575. https://doi.org/10.5194/angeo-20-1559-2002

Wolf, R. A., Wan, Y., Xing, X., Zhang, J.-C., & Sazykin, S. (2009). Entropy and plasma sheet transport. *Journal of Geophysical Research*, *114*, A00D05. https://doi.org/10.1029/2009JA014044

Wu, P., & Shay, M. A. (2012). Magnetotail dipolarization front and associated ion reflection: Particle-in-cell simulations. *Geophysical Research Letters*, *39*, L08107. https://doi.org/10.1029/2012GL051486

Wu, T., Fu, S. Y., Zong, Q. G., Sun, W. J., Cui, Y. B., Zhao, D., et al. (2016). Thin energetic O^+ layer embedded in the magnetotail reconnection current sheet observed by Cluster. *Geophysical Research Letters*, *43*, 11,493–11,500. https://doi.org/10.1002/2016GL071184

Yang, J., Toffoletto, F. R., Wolf, R. A., & Sazykin, S. (2011). RCM-E simulation of ion acceleration during an idealized plasma sheet bubble injection. *Journal of Geophysical Research*, *116*, A05207. https://doi.org/10.1029/2010JA016346

Yao, Z., Sun, W. J., Fu, S. Y., Pu, Z. Y., Liu, J., Angelopoulos, V., et al. (2013). Current structures associated with dipolarization fronts. *Journal of Geophysical Research: Space Physics*, *118*, 6980–6985. https://doi.org/10.1002/2013JA019290

Zhao, D., Fu, S. Y., Sun, W. J., Parks, G. K., Zong, Q. G., Shi, Q. Q., et al. (2016). Electromagnetic disturbances observed near the dip region ahead of dipolarization front. *Geophysical Research Letters*, *43*, 3026–3034. https://doi.org/10.1002/2016GL068033

Zhao, S. J., Fu, S. Y., Sun, W. J., Parks, G. K., Zhou, X. Z., Pu, Z. Y., et al. (2018). Oxygen ion reflection at earthward propagating dipolarization fronts in the magnetotail. *Journal of Geophysical Research: Space Physics*, *123*, 6277–6288. https://doi.org/10.1029/2018JA025689

Zhou, M., Ashour-Abdalla, M., Deng, X., Schriver, D., El-Alaoui, M., & Pang, Y. (2009). THEMIS observation of multiple depolarization fronts and associated wave characteristics in the near-Earth magnetotail. *Geophysical Research Letters*, *136*, L20107. https://doi.org/10.1029/2009GL040663

Zhou, M., Deng, X., Ashour-Abdalla, M., Walker, R., Pang, Y., Tang, C., et al. (2013). Cluster observations of kinetic structures and electron acceleration within a dynamic plasma bubble. *Journal of Geophysical Research: Space Physics*, *118*, 674–684. https://doi.org/10.1029/2012JA018323

Zhou, X.-Z., Angelopoulos, V., Liu, J., Runov, A., & Li, S.-S. (2014). On the origin of pressure and magnetic perturbations ahead of dipolarization fronts. *Journal of Geophysical Research: Space Physics*, *119*, 211–220. https://doi.org/10.1002/2013JA019394

Zhou, X.-Z., Angelopoulos, V., Sergeev, V. A., & Runov, A. (2010). Accelerated ions ahead of earthward-propagating dipolarization fronts. *Journal of Geophysical Research*, *115*, A00I03. https://doi.org/10.1029/2010JA015481

Zhou, X.-Z., Angelopoulos, V., Sergeev, V. A., & Runov, A. (2011). On the nature of precursor flows upstream of advancing of dipolarization fronts. *Journal of Geophysical Research*, *116*, A03222. https://doi.org/10.1029/2010JA016165

Zhou, X.-Z., Runov, A., Angelopoulos, V., Artemyev, A. V., & Birn, J. (2018). On the acceleration and anisotropy of ions within magnetotail depolarizing flux bundles. *Journal of Geophysical Research: Space Physics*, *123*, 429–442. https://doi.org/10.1002/2017JA024901